Extreme hyperallometry of mammalian antibacterial defenses

Cynthia J. Downs[1*], Laura A. Schoenle[2]†, Samantha J. Oakey[2], Ray Ball[3], Rays H.Y. Jiang[2], Kirk C. Klasing[4], Lynn B. Martin[2]

[1] Department of Environmental and Forest Biology, State University of New York College of Environmental Science and Forestry, Syracuse, NY 13210 USA

[2] Global and Planetary Health, University of South Florida, Tampa, FL 33620 USA

[3] Department of Biology, Eckerd College, Saint Petersburg, Florida 33711 USA

[4] Department of Animal Science, University of California, Davis, California 95616 USA

*Correspondence to: cjdowns@esf.edu

† Current address: Office of Undergraduate Biology, Cornell University, Ithaca, NY 14853 USA

Abstract: Terrestrial mammals span 7 orders of magnitude in body size, ranging from the < 2 g pygmy shrew (*Suncus etruscus*) to the > 3900 kg African elephant (*Loxodonta africana*). Although body size has profound effects on the behavior, physiology, ecology, and evolution of animals, how body mass affects immune functions is unknown. Here, using data from >160 terrestrial species of mammals, we show that the size-scaling of antibacterial activity in serum exhibits extreme hyperallometry. Compared to small mammals, the serum of large mammals is remarkably inhospitable to bacteria. Such hypermetric scaling of immune defenses provides novel perspectives on the ecology of host-pathogen interactions, and on their co-evolutionary dynamics. These results also have implications for effectively modeling human immunity and for identifying reservoirs of zoonotic pathogens.

Hosts can be thought of as islands whose size impacts how many parasites, including microbes can colonize them (*1*). Unsurprisingly, bigger hosts represent bigger islands, leading parasite abundance (*2*), biomass (*3*), diversity (*4*), size (*5*), size diversity (*6*), and prevalence (*7*) all to increase with host body size. Body size is also intimately connected to the relative value of self-defense versus reproduction (*8*), as most hosts reach large size via a long lifespan (*9*, *10*). Subsequently, natural selection should favor robust immune systems in large hosts, but physical or metabolic constraints could prevent the largest hosts from evolving optimal defenses. Eco-evolutionary processes are known to shape the architecture of species' immune systems (*11*, *12*), but whether body size constrains host immunity is little studied.

Generally, body size scaling relationships are modeled as power laws, $Y = a\,M^b$, with linear transformations, $\log_{10} Y = \log_{10} a + b \log_{10} M$, where Y is the focal trait, M is body mass, a is the intercept, and b is the scaling factor. To date, the Protecton and the Complexity of Immunity Hypotheses have received the most attention. Both frameworks predict that immunity should scale in direct proportion to body size (i.e., isometrically), which results in a mass-invariant relationship ($b = 0$) for concentrations (*13*, *14*). The fractal nature of the circulatory and lymphatic systems was argued to predict isometry because rates of parasite detection and delivery of defenses should be driven by transit of cells and proteins through the vasculature (*14–16*). By contrast, the Rate of Metabolism Hypothesis predicts a hypometric coefficient for immunity ($b < 0$ for a concentration) because all cell activities are linked to basal metabolic rates (BMR) (*17*). As mass-specific BMR scales at $b = -0.25$, immune defenses involving cell turnover and metabolism should scale similarly (*18*). Indirectly, some evidence supports this hypothesis (*19*); the causative agents of West Nile, rabies, and Lyme disease replicate more slowly in large host species (*20*), as do endogenous retroviruses over evolutionary time (*21*).

The Safety Factor Hypothesis, our focal hypothesis here, invokes performance-safety relationships from biophysics (*10*) and physiology (*22*), positing that large species should evolve disproportionately stronger (i.e., hypermetric, $b > 0$ for concentrations) damage-mitigation mechanisms than small ones (*9*, *10*). Immunologically, large hosts should thus evolve exceptionally robust constitutive defenses to protect against the greater infection risks they will experience. Variants of the Safety Factor Hypothesis exist in the literature already, including Peto's paradox for cancer (*23*) and optimal defense theory (*24*). Only recently, however, has direct empirical evidence been provided for immune defenses, namely hypermetric scaling for neutrophil concentrations in mammals ($b = 0.11$) (*9*) and heterophil concentrations in birds ($b = 0.19$) (*25*).

The limitation of these and most immune allometry studies is how to interpret them. Hypermetric scaling of cell concentrations could represent greater protection in large animals or simply evidence that large animals must compensate for lower per-cell effectiveness in combatting infections by circulating more cells. Cell size scales isometrically but per-gram metabolism scales hypometrically (*26*), so the average large-animal leukocyte might be comparatively ineffective compared to a leukocyte from a small species. Moreover, as selection tends to act on integrated traits (*27*), scaling inference based on processes that affect host fitness will inherently be more insightful. Few scaling studies of immunity to date have relied on integrated immune functions, and others either involved few species or found body mass effects but did not estimate allometries (*9*).

Our goals here were i) to determine how blood-based antibacterial defenses scaled with body size among terrestrial mammals, and ii) to test whether the Safety Factor hypothesis best-

predicts the scaling exponent ($b > 0$) for this type of immunity. We focused on the antibacterial capacity of sera (*28*), as this defense is an important determinant of host health and virulence for certain bacterial pathogens (*29*), as well as measurable in a standard, reagent-independent way among diverse species. Briefly, antibacterial capacity measures bacteriostasis and bacteria killing capacity of sera. To describe interspecific variation in this immune function in the most confound-free manner possible, we compared the efficacy of sera of several, independent replicates from adults of mammalian species housed in zoos. To provide generality to any scaling we observed, we quantified the antibacterial capacity of sera of 160+ mammalian species against three distinct bacteria, *Escherichia coli* (ATCC #8739), *Salmonella enterica* (ATCC #13311), and *Micrococcus luteus* (ATCC # 4698) (*28*). These bacteria are common pathogens of many vertebrates, some portion of their natural infection timeline occurs in blood (*30*), and they are controlled effectively by blood-borne immune defenses (*29*). As their last common evolutionary ancestor was ancient, any consistency in allometries for the antibacterial capacity against these particular bacteria should be more attributable to host immunity than parasite phylogenetic history.

Results: Scaling of antibacterial capacity

To describe constitutive, antibacterial immunity, we fit non-linear functions to 12-step sera dilution series data from each individual animal with extensive individual-level replication across mammalian species (n = 1-67 replicates per species, mean = 5, Fig. S1) (*31*). We characterized antibacterial dilution series, instead of antibacterial capacity at single dilutions, as the shapes of resultant *ex vivo* antibacterial functions capture salient aspects of defense (Fig. 1A). For instance, if a very dilute serum sample was effective against a standard amount of bacteria, an animal of that host species would be relatively adept at controlling a large initial dose of bacteria in its bloodstream. Other meaningful antibacterial parameters included i) the maximum amount of bacteria that serum could protect against, ii) the serum dilution at the point of most rapid change from protected to vulnerable, and iii) the slope at this steepest part of the antibacterial function. This last parameter could be a proxy for either how rapidly serum defenses could be recruited to a bacterial replication event (*32*) or capture the pattern by which proteins and other molecules were recruited combinatorically to control bacteria. The Safety Factor hypothesis, our focal hypothesis, predicts that larger mammals will have higher maximal antibacterial capacity, higher antibacterial capacity at a specific dilution, and a more rapid shift from vulnerable to complete protection (Fig. 1B).

To identify any allometries, we first fit non-linear antibacterial functions for each individual separately, then analyzed curve parameters as response variables in a set of multivariate, mixed-effects models (one for each bacterium) (*31*). This approach allowed us to estimate the scaling coefficients for several aspects of each antibacterial function while simultaneously accounting for potential correlations among antibacterial curve elements as well as inter- and intra-specific variation (*33*). To check whether antibacterial data were affected by the shared evolutionary history of host species, we also generated a separate set of phylogenetic univariate mixed-effects models (*31*). We built separate models for each curve parameter with all other curve parameters and body mass included as fixed effects. We estimated a phylogenetic covariance matrix using a tree constructed with National Center for Biotechnology Information molecular data and phyloT (Fig. S2) (*34*). Overall, phylogeny explained little variation (Table S1), so we do not address it further.

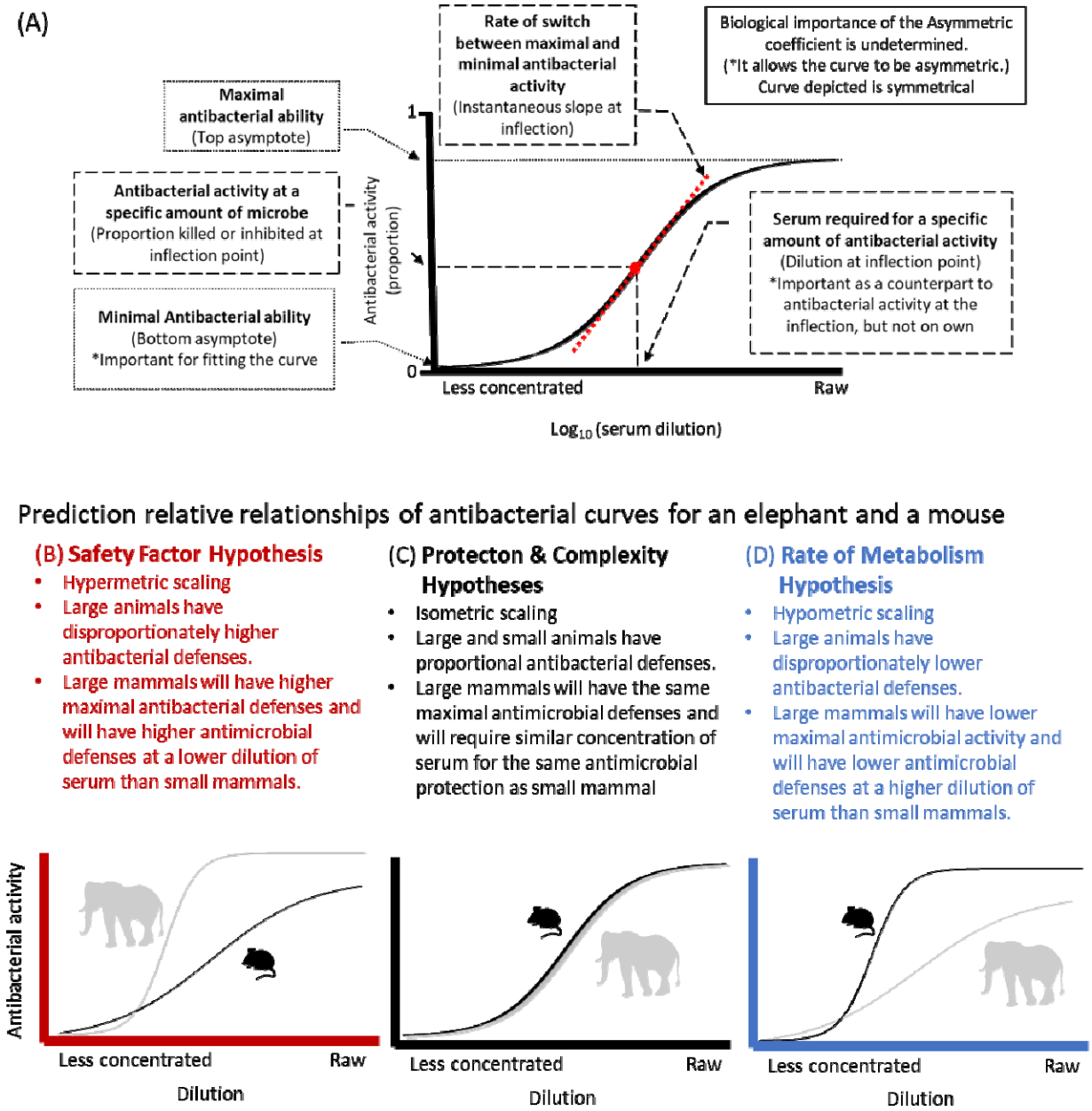

Figure 1. Antibacterial capacity dilution curves support the Safety Factor hypothesis. Hypothetical antibacterial dilution curve showing the parameters we estimated and biological interpretation (A). Hypothetical antibacterial curves for an elephant and mouse showing predictions for the Safety Factory Hypothesis (B), the Protecton and Complexity Hypotheses (C), and Rate of Metabolism Hypothesis (D).

Our results strongly support the Safety Factor Hypothesis (Table 1). In general, results for antibacterial capacity against *E. coli*, *S. enterica*, and *M. luteus* are qualitatively similar (Table 1). Mammalian species had diverse antibacterial curves (Movie S1). Even with this diversity, large species were much better able to control bacteria than small species and had

higher antibacterial capacity overall (Fig. 2). Large species required less serum to obtain the same antibacterial capacity, had a higher maximal antimicrobial capacity, and more steeply escalated antibacterial capacity over a shorter range of serum dilutions (Table 1, Fig S4). Large mammals also exhibited generally steeper transitions from minimal to maximal protection (Fig. 2A); one of the smallest species, the cotton mouse (*Peromyscus gossypinus*), exhibited a gradual decline in the efficacy of antibacterial capacity against *E. coli* whereas the largest species, the Asian elephant (*Loxodonta africana*), continued to have complete protection even with very dilute sera (Fig. 2B). Importantly, *b* for most dilution series parameters scaled hypermetrically for all three bacteria (Table 1). Although the directions of allometries were consistent among bacteria and curve parameters, the magnitude of the slope at the steepest part of the antibacterial functions were quite distinct. For this particular parameter, allometric effects were weak for *M. luteus* (b = 2.4), strong for *S. enterica* (b = 5.2), and extreme for *E. coli* (b = 8.7; Fig. S3 A-C).

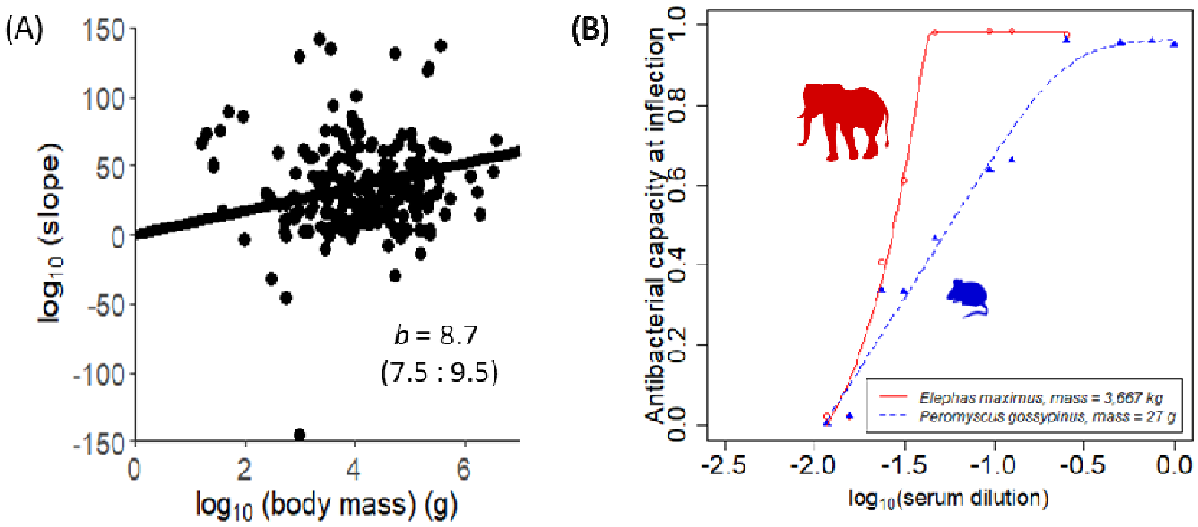

Figure 2. *Antibacterial capacity dilution curves support the Safety Factor Hypothesis. Larger species have curves with disproportionately steeper slopes at the instantaneous inflection point of the antibacterial curve against Escherichia coli (A, each point represents a species mean, but analyses were performed on individual-level data). A representative curve for a large species, Asian elephant (3100 kg) and a small species, cotton mouse (25 g, C) demonstrate the general pattern that larger species had higher antibacterial capacity overall (B). Asian elephants have higher maximal capacity, required less serum to obtain the same capacity, and shift more rapidly from minimal to maximal antibacterial capacity.*

Discussion: Antibacterial capacity scale hypermetrically

Our data provide strong evidence for hypermetric scaling of serum antibacterial activity in terrestrial mammals. Hypermetric antibacterial activity might have evolved because large species face greater risk of infection and have more to lose evolutionarily from disease than small species. However, large species have more resources (i.e., space and energy density) on which parasites can capitalize (*35*), so we cannot rule out that parasites might sometimes be

selected to infect large species. On the other hand, small species provide many more transmission opportunities for many parasites given the comparatively greater densities of small hosts (*36*). The forces that lead to immune allometries warrant future investigation, and below we propose briefly some ideas for why and how antibacterial immunity among mammals scales hypermetrically.

Why do antibacterial defenses scale hypermetrically?

The evolution of the vertebrate adaptive immune system (and its functional equivalents) enabled chordates to solve perhaps one of the most perplexing problems of life: how to detect an infinite diversity of enemy markers (i.e., antigens and pathogen-associated molecular patterns) with a limited set of protein-coding genes. Clearly, not only are vertebrates and their immediate ancestors adept at this task, but B and T cell receptor diversity is more constrained by over-responsiveness to self- than under-responsiveness to non-self (*37*). Indeed, the probability that a parasite will evade the antigen space covered by B and T cell repertoires is $4x10^{-44}$ (*15*, *38*). Adaptive immune systems will therefore eventually detect any antigen that ever evolves. The challenge of relying solely on these defenses, though, is that they involve major time lags (i.e., minimally 4-10 days but perhaps longer if the immune system is still developing (*39*)). Lags for inducible defenses generally leave hosts vulnerable as microbial doubling time proceeds over much shorter period. This incompatibility might explain why among 25 avian species, the production rate of infectious virions and the burst size of cells (i.e., the number of infectious virions released by an infected cell over its infected lifespan) scaled hypometrically, yet the rate of antibody-mediated neutralization of virus was isometric (*15*). Perhaps hypermetrically-scaled constitutive immune defenses produced the surprisingly low viral outcomes observed in that study.

We expect that hypermetric immune allometries are likely pervasive in the first, constitutive lines of host defense. When parasites grow rapidly, as bacterial (and viral) infections often do, defenses with short time-delays are favored (*24*). Barriers against all-comers are the best option when adversaries can replicate faster than defenses can be honed and mobilized. The downside to these forms of defense is that they impose comparatively large costs, especially when adversaries are absent (*40*). Recently, a meta-analysis revealed that small animal species that are relatively long-lived incur the greatest costs of *induced* immune defenses (*41*). Given their tendency to breed prolifically and develop rapidly, hypermetric allometries might manifest as much because small species favor rapidly-mobilizable defenses that are activated only after exposure to a parasite as they do because of mandates of large size.

Mechanisms of hypermetric scaling.

Another conspicuous opportunity in light of our findings is to resolve how large mammals achieve hypermetric antibacterial capacity. We expect (but could not measure) that complement and other circulating proteins (i.e., lysozyme, mannan-binding protein, beta-defensins) mediate most of what we quantified. Complement provides protection against diverse bacteria via three pathways, but here the alternative complement pathway is implicated because we used serum for assays (*32*). Large animals might achieve higher antibacterial capacity because they mobilize pathways more rapidly, assemble functional membrane attack proteins

more swiftly, or maintain higher concentrations of particular immune proteins. For example, large species may express more of a key complement element, C3, and disproportionately more decay-accelerating factor, CD55, or Factors H or B to minimize any detrimental effects of high C3 activity (*32*). Factor D might also be a critical step in the pathway because it circulates in an active form whereas the others circulate as zymogens (*32*). Alternatively, these patterns might arise in part because of trade-offs between the various functional responsibilities of the blood and liver. Many of the constitutive proteins involved in the antibacterial defenses we measured in serum are produced in the liver (*42*). The liver also exports proteins, glucose, and lipoproteins to support cellular maintenance and respiration, among other important functions. The high mass-specific metabolic rates rate of small animals and consequent high demand for these hepatic inputs may limit the liver's capacity to produce antibacterial proteins. Additionally, there is a direct relationship between the amount of protein in the blood and its viscosity (*43*). This limits the amount of protein that blood can transport because increased viscosity decreases microvascular perfusion and delivery of nutrients and oxygen to cells. The high mass-specific metabolic rate of small animals results in the challenge of needing to deliver more nutrients and oxygen to cells without increasing blood viscosity, which may result in lower concentrations of antibacterial proteins (*44*), although this perspective would not explain why large species would be so adept at antibacterial defense. In the future, it would be interesting to reveal why the magnitude of antibacterial allometries varied among bacterial species. Whereas *M. luteus* grows slowly and causes modest disease relative to the other two bacteria, both *S. enterica* and *E. coli* can cause sepsis (*45*), infect via the diet, and have similar replication rates in culture. The scaling disparities we detected (Table 1) suggest that risk of morbidity or death to *E. coli* is enhanced relative to the other two bacteria, but too few data on sepsis yet exist and too many interspecific disparities remain to resolve this issue (*46*, *47*).

Why should we care?

Our findings have ramifications for human medicine and management of disease cycles, especially zoonoses. In regard to medicine, we might revisit how we choose species as models of human immunity (*48*). One option is to use the scaling effects described here as a form of null model from which to extrapolate currently favored rodent species responses to human applications. A greater understanding of immune scaling could also help develop better epidemiological models. Because "the rate that pathogens spread through populations is influenced by the rate of spread through individual hosts" (*49*), we must understand better how host traits affect their propensity to maintain and transmit viable parasites (*50*, *51*).

We expect that many more important immune allometries await description, and in particular, we encourage future scaling work on Order *Chiroptera*, as bats are implicated in the emergence of many zoonoses including SARS-COV2 (*52*, *53*). Unfortunately, bats are rare in zoos, so few bat species were in our analysis. We also encourage efforts to investigate immune allometries in ectotherms, and especially vectors, as their immune defenses are more temperature-dependent (*17*), an important condition for a planet undergoing extensive climate change. We also hope creative approaches can be applied to scaling studies of more pathogenic microbes, ideally in more organismal contexts. Such work is challenging, as pathogenicity differs among species as well as route of infection (*29*). By continuing to merge cellular and molecular efforts with the behavioral, ecological, and evolutionary concepts, we can produce a

more integrative immunology and thus more effective options to predict and manage infectious disease risk.

Materials and Methods

Samples. We used the simulations performed by Dingemanse and Dochtermann to guide our sample sizes (*Fig. 1 of 33*). We obtained serum from 212 species of healthy, zoo- and lab-housed animals ranging in body size from 16 g – 3,600 kg, which covers the range of body sizes of extant terrestrial mammals (Fig. S4) (*54*). Most zoo samples were collected as part of routine wellness checkups whereas lab samples were collected at the termination of experiments. We supplemented zoo samples, which comprised the vast majority, with samples from lab-housed animals to augment small-bodied species (< 2 kg) in our analysis, which are rare in most zoos. We could not run all assays against all bacterial species for all samples because of sample volumes. Final sample sizes of species were 212, 199, and 167 for antibacterial capacity against *E. coli*, *S. enterica*, and *M. luteus*, respectively. We assayed a mean of 5 samples per species for each microbe (Fig. S1). We also obtained >15 samples from a subset of species representing the full range of body masses to help ensure that a single individual from a large or small species was not leveraging results (Fig. S5) Samples were stored at the collection location at -80 to -20 °C until shipped on dry ice to USF or Hamilton College where they were stored at 80°C until assays. Samples were used in assays within 24h of thawing. We restricted our analysis to samples collected in the years 2005-2019 because preliminary work indicated that samples collected before 2005 had reduced antibacterial ability. Use of these samples was approved by the Institutional Animal Care and Use Committees at Hamilton College (memo of understanding), SUNY ESF (memo of understanding), and University of South Florida (Protocol # 4920).

Antibacterial capacity. We measured antibacterial capacity against *E. coli* (ATCC #8739), *S. enterica* (ATCC #13311), and *M. luteus* (ATCC # 4698) using an adaptation of the microbiocidal assay (a.k.a. bacteria killing assay, BKA, microbiocidal activity) developed by French and Neuman-Lee (*28*). Briefly, we plated a 12-point dilution curve of each animal sample in triplicate on a round-bottomed 96-well plate. *E. coli* had two serial dilutions: 6 points from raw to 1:64, and 6 points from 3:4 to 3:256. *S. enterica* also had two serial dilutions: 6 points from raw to 1:64, and 6 points from 3:4 to 3:128. *M. luteus* had a single serial dilution ranging from raw serum to 1:2048. Super antibacterial capacity curves—curves for species with 100% antibacterial capacity at the lowest dilution of the normal curves—for *E. coli* were 6 points from 1:4 to 1:256 and 6 points from 3:16 to 3:512 and for were *S. enterica*: 6 points from 1:16 to 1:512 and 6 points from 3:4 to 3:128. We also plated a 4-point dilution curve in Dulbecco's Phosphate Buffered Saline (PBS, Sigma-Aldrich #D8537) of commercially available cow serum (Innovative Research Novi, MI 48377, #IBV-Compl) as our inter-assay control. Cow curve dilutions were 1:32, 1:64, 1:128, 1:256 for *E. coli*; 1:16, 1:32, 1:64, 1:128 for *S. enterica*; and 1;20, 1:80, 1:320, 1:1280 for *M. luteus*. Our final volume of each serum dilution was 18 µl. We plated three replicates of a 20 µl negative control of PBS and 9 replicates of an 18 µl positive control. We added 2 µl of a standard concentration (10^4 CFU ml^{-1}) of bacteria to all wells except the negative controls. We incubated plates for 30 min. at 37 °C. We next added 125 µl of tryptic soy broth (BD #211825) to all wells, and then shook the plate for 1 min at 300 rpm. We then

measured baseline absorbance of all wells at 300 nm using a plate reader (Biotek Synergy HTX Multi-Mode Reader) to serve as an internal control. We incubated the covered plate for 12 h for *E. coli*, 10 h for *S. enterica*, and 48 h for *M. luteus* at an incubation temperature of 37 °C. We measured final absorbance of all wells again at 300 nm. Antibacterial capacity for each well was calculated as $\left(1 - \frac{mean(sample\ end - sample\ baseline)}{mean(positive\ control\ start - positive\ control\ end)}\right) * 100\%$. We observed little evidence of sample degradation due to preservation method or duration, nor did we observe high inter-assay (9.02%) or intra-assay variation (0.02%). Key parameters of the antibacterial capacity assay for each microbe are summarized in Table S1 and full details about the procedures used to develop and validate our assays are available in the Supplementary Text. Assay protocols are deposited on FigShare (*55*).

Data processing and analysis. Statistics were analyses using protocols in Program R (*56*). We compiled data using a workflow developed using Program R (*62*) (all code files are available on Figshare (*57*)). We visually checked each sample dilution curve for outliers (i.e., replicates that were distinct from the other two replicates and/or fell off the expected sigmoidal curve). We determined whether positive controls, negative controls, and inter-assay controls (i.e., cow sera) were within the expected range, and discarded the plate if data fell outside expected ranges. To determine how antibacterial capacity (i.e., the shape of dilution curves across all 12-serum concentrations) scaled with body mass, we fit 5-parameter logistic regression growth curves to the cleaned dilution curves for each sample using package *nplr* (*58*). To aid in curve-fitting, we $\log_{10}$-transformed serum concentrations (i.e., the dilutions) and converted the antibacterial ability from a percent to a proportion. Curves could only be fit to values between 0 and 1, so percent inhibited values > 100 were forced to a random value between 99 and 100 and percent inhibited values < 0 were forced to a random value between 0 and 1 prior to conversion to proportions. This approached restricted values to a range near maximal and minimal antibacterial activity for all other curves. We extracted the curve parameters ($\text{inflection}_{\text{dilution}}$, $\text{inflection}_{\text{antibacterial capacity}}$, bottom $\text{asymptote}_{\text{antibacterial capacity}}$, top $\text{asymptote}_{\text{antibacterial capacity}}$, slope, asymptote coefficient) for use in univariate and multivariate general linear models (Fig. 1A). Slope and $\text{inflection}_{\text{dilution}}$ were already on $\log_{10}$-scale. We added 1 to $\text{Inflection}_{\text{antibacterial capacity}}$, bottom $\text{asymptote}_{\text{antibacterial capacity}}$, top $\text{asymptote}_{\text{antibacterial capacity}}$ and then $\log_{10}$-transfromed them. We also $\log_{10}$-transformed body mass. All analyses were performed using transformed data.

To check for effects of mammalian phylogeny on antibacterial capacity, we constructed a separate phylogenetic univariate mixed model for each curve parameter for each bacterium. We included body mass and all other curve parameters as fixed effects then fit models using MCMCglmm (*59, 60*). The phylogenetic covariance matrix for this analysis was estimated using a phylogenetic tree constructed with NCBI molecular data and phyloT (Fig S2) (*40*). All mixed models were fit using a weak inverse-Gamma prior with shape and scale parameters set to 0.01 for the random effect of phylogenetic variance. Default priors for all other fixed effects were used. Model chains were run for 7.8×10^5 iterations, with an 180,00-iteration burn-in and a 600-iteration thinning interval. We estimated Pagel's lambda as a measure of how much of the total observed variation was explained by phylogeny (61).

Once strong effects of phylogeny were ruled out, we generated separate multivariate mixed models to query body mass effects on antibacterial capacity. Log_{10}-transformed body mass was included as a fixed effect and species was included as a random effect. This model

allowed species to have different intercepts and slopes. These models were fit using the MCMCglmm package (*59, 60*). All mixed models were fit using a weak inverse-Gamma prior with shape and scale parameters set to 1.002 for the random effect. Default priors for all other fixed effects were used. Model chains were run for 1.82×10^6 iterations, a 420,000-iteration burn-in, and a 1400 iteration thinning interval. Results were robust across alternative priors, and chain length was sufficient to yield negligible autocorrelation. We extracted the slopes describing the relationship between each parameter and body mass across all species.

We included bacterial capacity at the bottom $\text{asymptote}_{\text{antibacterial capacity}}$ and asymmetric coefficient in our models because they helped describe antibacterial capacity curves although we did not make predictions about their biological functions. In our study, we did not always collect data at the lower asymptote because we limited our sampling to 12-dilutions. As a result, the bottom asymptote estimated by the general linear model was based on incomplete data and not biologically relevant to our scaling hypotheses. The dilution at the inflection point was also include in our models because it informed our understanding of the antibacterial capacity at the inflection point, but it was not biologically meaningful for testing scaling of immune defenses by itself. Results for these parameters can be found in Table S2.

References (including those for supplemental materials):

1. A. M. Kuris, A. R. Blaustein, J. J. Alio, Hosts as islands. *Am Nat*. **116**, 570–586 (1980).

2. T. L. Kieft, K. A. Simmons, Allometry of animal–microbe interactions and global census of animal-associated microbes. *Proc. R. Soc. B*. **282**, 20150702 (2015).

3. R. Poulin, M. George-Nascimento, The scaling of total parasite biomass with host body mass. *International Journal for Parasitology*. **37**, 359–364 (2007).

4. V. O. Ezenwa, Interactions among host diet, nutritional status and gastrointestinal parasite infection in wild bovids. *International Journal for Parasitology*. **34**, 535–542 (2004).

5. L. Harrison, Mallophaga from *Apteryx* , and their Significance; with a Note on the Genus *Rallicola*. *Parasitology*. **8**, 88–100 (1915).

6. R. Poulin, *Evolutionary ecology of parasites* (Princeton University Press, Princeton, NJ, 2007).

7. F. Ishtiaq, C. G. R. Bowden, Y. V. Jhala, Seasonal dynamics in mosquito abundance and temperature do not influence avian malaria prevalence in the Himalayan foothills. *Ecol Evol*. **7**, 8040–8057 (2017).

8. W. A. Calder III, *Size, function, and life history* (Dover Publications, Mineola, NY, 1984).

9. C. J. Downs, N. A. Dochtermann, R. Ball, K. C. Klasing, L. B. Martin, The Effects of Body Mass on Immune Cell Concentrations of Mammals. *The American Naturalist*. **195**, 107–114 (2020).

10. J. F. Harrison, Do Performance–Safety Tradeoffs Cause Hypometric Metabolic Scaling in Animals? *Trends in Ecology & Evolution*. **32**, 653–664 (2017).

11. B. C. Sheldon, S. Verhulst, Ecological immunology: costly parasite defences and trade-offs in evolutionary ecology. *Trends in Ecology & Evolution*. **11**, 317–321 (1996).

12. C. J. Downs, J. S. Adelman, G. E. Demas, Mechanisms and Methods in Ecoimmunology: Integrating Within-Organism and Between-Organism Processes. *Integrative and Comparative Biology*. **54**, 340–352 (2014).

13. R. E. Langman, M. Cohn, The E-T (Elephant-Tadpole) paradox necessitates the concept of a unity of B-cell function: The protecton. *Molecular Immunology*. **24**, 675–697 (1987).

14. F. W. Wiegel, A. S. Perelson, Some Scaling Principles for the Immune System. *Immunol Cell Biol*. **82**, 127–131 (2004).

15. S. Banerjee, A. S. Perelson, M. Moses, Modelling the effects of phylogeny and body size on within-host pathogen replication and immune response. *J. R. Soc. Interface*. **14**, 20170479 (2017).

16. S. Banerjee, A mathematical framework for understanding how lymph node architecture scales with host body size to produce an efficient immune response, 8 (2018).

17. J. H. Brown, J. F. Gillooly, A. P. Allen, V. M. Savage, G. B. West, Toward a Metabolic Theory of Ecology. *Ecology*. **85**, 1771–1789 (2004).

18. D. Dingli, J. M. Pacheco, Allometric Scaling of the Active Hematopoietic Stem Cell Pool across Mammals. *PLoS ONE*. **1**, e2 (2006).

19. C. J. Downs, L. A. Schoenle, B. A. Han, J. F. Harrison, L. B. Martin, Scaling of Host Competence. *Trends in Parasitology*. **35**, 182–192 (2019).

20. J. M. Cable, B. J. Enquist, M. E. Moses, The Allometry of Host-Pathogen Interactions. *PLoS ONE*. **2**, e1130 (2007).

21. A. Katzourakis, G. Magiorkinis, A. G. Lim, S. Gupta, R. Belshaw, R. Gifford, Larger Mammalian Body Size Leads to Lower Retroviral Activity. *PLoS Pathog*. **10**, e1004214 (2014).

22. J. Diamond, Quantitative evolutionary design. *The Journal of Physiology*. **542**, 337–345 (2002).

23. R. Peto, in *Origins of human cancer*, J. D. Watson, H. H. Hiatt, J. A. Winsten, Eds. (Cold Spring Harbor Laboratory, New York, NY, 1977), pp. 1403–1428.

24. E. Shudo, Y. Iwasa, Inducible Defense against Pathogens and Parasites: Optimal Choice among Multiple Options. *Journal of Theoretical Biology*. **209**, 233–247 (2001).

25. E. Cornelius Ruhs, L. B. Martin, C. J. Downs, The impact of body mass on immune cell concentrations in birds. *bioRxiv* (2020), doi:10.1101/2020.04.23.057794.

26. K. Schmidt-Nielsen, *Scaling: why is animal size so important?* (Cambridge University Press, Cambridge, 1984).

27. A. F. Bennett, R. B. Huey, Studying the evolution of physiological performance. *Oxford surveys in evolutionary biology*. **7**, 251–284 (1990).

28. S. S. French, L. A. Neuman-Lee, Improved ex vivo method for microbiocidal activity across vertebrate species. *Biology Open*. **1**, 482–487 (2012).

29. P. W. Taylor, Bactericidal and bacteriolytic activity of serum against gram-negative bacteria. *Microbiological Reviews*. **47**, 46–83 (1983).

30. H.-W. Mittrücker, S. H. E. Kaufmann, Immune response to infection with *Salmonella typhimurium* in mice. *J Leukoc Biol*. **67**, 457–463 (2000).

31. Materials and Methods Section.

32. K. P. Murphy, P. Travers, M. Walport, *Janeway's immunobiology*. (Garland Science, New York, ed. 7th, 2007).

33. N. J. Dingemanse, N. A. Dochtermann, Quantifying individual variation in behaviour: mixed-effect modelling approaches. *J Anim Ecol*. **82**, 39–54 (2013).

34. I. Letunic, *phyloT: phylogenetic tree generator*. (2015; http://phylot .biobyte.de.).

35. R. F. Hechinger, A Metabolic and Body-Size Scaling Framework for Parasite Within-Host Abundance, Biomass, and Energy Flux. *The American Naturalist*. **182**, 234–248 (2013).

36. R. S. Ostfeld, T. Levi, A. E. Jolles, L. B. Martin, P. R. Hosseini, F. Keesing, Life History and Demographic Drivers of Reservoir Competence for Three Tick-Borne Zoonotic Pathogens. *PLoS ONE*. **9**, e107387 (2014).

37. R. J. De Boer, A. S. Perelson, How diverse should the immune system be? *P Roy Soc B-Biol Sci*. **252**, 171–175 (1993).

38. A. S. Perelson, G. Oster, Theoretical Studies of Clonal Selection: Minimal Antibody Repertoire Size and Reliability of Self-Non-self Discriminationt. *Journal of Theoretical Biology*. **81**, 645–670 (1979).

39. R. E. Ricklefs, Embryonic development period and the prevalence of avian blood parasites. *Proceedings of the National Academy of Sciences*. **89**, 4722–4725 (1992).

40. M. W. Sears, J. P. Hayes, C. S. O'Connor, K. Geluso, J. S. Sedinger, Individual variation in thermogenic capacity affects above-ground activity of high-altitude Deer Mice. *Funct Ecology*. **20**, 97–104 (2006).

41. A. J. Brace, M. J. Lajeunesse, D. R. Ardia, D. M. Hawley, J. S. Adelman, K. L. Buchanan, J. M. Fair, J. L. Grindstaff, K. D. Matson, L. B. Martin, Costs of immune responses are related to host body size and lifespan. *J. Exp. Zool*. **327**, 254–261 (2017).

42. Z. Zhou, M.-J. Xu, B. Gao, Hepatocytes: a key cell type for innate immunity. *Cell Mol Immunol*. **13**, 301–315 (2016).

43. H. C. Kwaan, Role of plasma proteins in whole blood viscosity: A brief clinical review. *Clinical Hemorheology and Microcirculation*. **44**, 167–176 (2010).

44. A. J. Hulbert, P. L. Else, Basal Metabolic Rate: History, Composition, Regulation, and Usefulness. *Physiological and Biochemical Zoology*. **77**, 869–876 (2004).

45. T. van der Poll, S. M. Opal, Host–pathogen interactions in sepsis. *The Lancet Infectious Diseases*. **8**, 32–43 (2008).

46. M. P. Fink, Animal models of sepsis. *Virulence*. **5**, 143–153 (2014).

47. D. Rittirsch, L. M. Hoesel, P. A. Ward, The disconnect between animal models of sepsis and human sepsis. *Journal of Leukocyte Biology*. **81**, 137–143 (2007).

48. C. L. Althaus, Of mice, macaques and men: scaling of virus dynamics and immune responses. *Front. Microbiol*. **6** (2015), doi:10.3389/fmicb.2015.00355.

49. G. A. De Leo, A. P. Dobson, Allometry and simple epidemic models for microparaites. *Nature*. **379**, 720–722 (1996).

50. L. Bolzoni, G. A. De Leo, M. Gatto, A. P. Dobson, Body-size scaling in an SEI model of wildlife diseases. *Theoretical Population Biology*. **73**, 374–382 (2008).

51. G. A. De Leo, A. P. Dobson, M. Gatto, Body size and meta-community structure: the allometric scaling of parasitic worm communities in their mammalian hosts. *Parasitology*. **143**, 880–893 (2016).

52. K. J. Olival, P. R. Hosseini, C. Zambrana-Torrelio, N. Ross, T. L. Bogich, P. Daszak, Host and viral traits predict zoonotic spillover from mammals. *Nature*. **546**, 646–650 (2017).

53. B. A. Han, A. M. Kramer, J. M. Drake, Global Patterns of Zoonotic Disease in Mammals. *Trends in Parasitology*. **32**, 565–577 (2016).

54. F. A. Smith, S. K. Lyons, How big should a mammal be? A macroecological look at mammalian body size over space and time. *Phil. Trans. R. Soc. B* **366**, 2364–2378 (2011).

55. L. A. Schoenle, L. B. Martin, C. J. Downs, Protocols for 12-dilution antibacterial capacity curves for interspecific comparisons. *Figshare* (2020). DOI:10.6084/m9.figshare.12501149.

56. R Core Team, *R: A language and environment for statistical computing* (R Foundation for Statistical Computing, 2019).

57. N. J. Keith, L. B. Martin, C. J. Downs, Code to compile data and analyzing data for a comparative antimicrobial analysis. figshare. (2020). DOI: 10.6084/m9.figshare.12430103.

58. F. Commo, B. M. Bot, R package nplr n-parameter logistic regressions. 11 (2016).

59. J. D. Hadfield, S. Nakagawa, General quantitative genetic methods for comparative biology: phylogenies, taxonomies and multi-trait models for continuous and categorical characters. *Journal of Evolutionary Biology* **23**, 494–508 (2010).

60. J. D. Hadfield, MCMC Methods for Multi-Response Generalized Linear Mixed Models: The **MCMCglmm** *R* Package. *J. Stat. Soft.* **33** (2010).

61. E. A. Housworth, E. P. Martins, M. Lynch, The Phylogenetic Mixed Model. *The American Naturalist* **163**, 84–96 (2004).

62. G. E. Demas, D. A. Zysling, B. R. Beechler, M. P. Muehlenbein, S. S. French, Beyond phytohaemagglutinin: assessing vertebrate immune function across ecological contexts: Assessing vertebrate immune function across ecological contexts. *Journal of Animal Ecology* **80**, 710–730 (2011).

63. K. D. Matson, A. A. Cohen, K. C. Klasing, R. E. Ricklefs, A. Scheuerlein, No simple answers for ecological immunology: relationships among immune indices at the individual level break down at the species level in waterfowl. *Proc. R. Soc. B* **273**, 815–822 (2006).

64. B. I. Tieleman, J. B. Williams, R. E. Ricklefs, K. C. Klasing, Constitutive innate immunity is a component of the pace-of-life syndrome in tropical birds. *Proc. R. Soc. B* **272**, 1715–1720 (2005)

Acknowledgments: We thank Birmingham Zoo, Busch Gardens Tampa Bay (Cara Martel), Cleveland Metroparks Zoo, Columbus Zoo, the Denver Zoological Foundation, Dickerson Park Zoo, Indianapolis Zoo, Lincoln Park Zoo, Louisville Zoological Garden, Maryland Zoo in Baltimore, Milwaukee County Zoo, Naples Zoo, Nashville Zoo at Grassmere, Oregon Zoo (Mitch Finegan & David Shepherdson), Sedgwick County Zoo, Smithsonian's National Zoo and Conservation Biological Institute, Topeka Zoo & Conservation Center, Zoo Atlanta (Hayley Murphy, Stephanie Earhardt), ZooTampa at Lowry Park, and the Demas (Indiana State University), Hoekstra (Harvard University), Ophir (Cornell University), Place (Cornell Univeristy), and Monteith (University of Wyoming) labs for donating serum samples. We thank M. Amy, B. Butler, K. Carlson, E. Chinchilli, K. Clausen, H. Droke, M. Espino, A. Fernandez, M. Galan, M. Henning, N. Huizenga, K. Koller, E. Lee, O. Ogunsina, V. Pappademetriou, A. Roberts, C. Stanell, S. Travis, A. Vorrath, R. Winner, C. Yeung for help with laboratory work. N. Keith helped develop the

Program R workflows required to process our data. We thank N.A. Dochtermann and J.C. Uyeda for statistical guidance, and the Martin Lab and HA Woods for discussion about an early version of the manuscript. **Funding:** This work was supported by State University of New York College of Environmental Science and Forestry's Provost Office, the Levitt Center, Hamilton College's Dean of Faculty Office, University of South Florida's College of Public Health, and the National Science Foundation (award numbers IOS 1656551 to C.J.D. and IOS 1656618 to L.B.M).; **Competing interests:** Authors declare no competing interests.

Supplementary Materials:

One file containing:

Supplementary Methods

Figures S1-S8

Tables S1-S3

Table 1. Allometric scaling coefficients for relevant antibacterial dilution curve parameters.

Bacteria	Response variable: Logistic curve parameter	Fixed effect: log_{10} body mass			Scaling type
		β estimate[1]	Effective sample	P	
Escherichia coli	$Inflection_{antibacterial\ capacity}$	0.185 (0.097 : 0.262)	1000	<0.001	hyper
	$Top\ asymptote_{antibacterial\ capacity}$	0.324 (0.258 : 0.44)	1000	<0.001	hyper
	Slope	8.656 (7.498 : 9.514)	1099	<0.001	hyper
Salmonella enterica	$Inflection_{antibacterial\ capacity}$	0.020 (0.008 : 0.036)	794.1	0.002	hyper
	$Top\ asymptote_{antibacterial\ capacity}$	0.045 (0.032 : 0.061)	819.3	<0.001	hyper
	Slope	5.159 (4.369 : 5.954)	1000	<0.001	hyper
Micrococcus luteus	$Inflection_{antibacterial\ capacity}$	0.004 (-0.016 : 0.022)	1000	0.832	iso
	$Top\ asymptote_{antibacterial\ capacity}$	0.016 (0.003 : 0.042)	1000	0.032	hyper
	Slope	2.418 (1.787 : 3.031)	920.6	<0.001	hyper

***** $Inflection_{antibacterial\ capacity}$ and top $Asymptote_{antibacterial\ capacity}$ were+1, log_{10}-transformed. Body mass and slope were log_{10}-transformed prior to beta estimation.
[1] mode ± credible interval